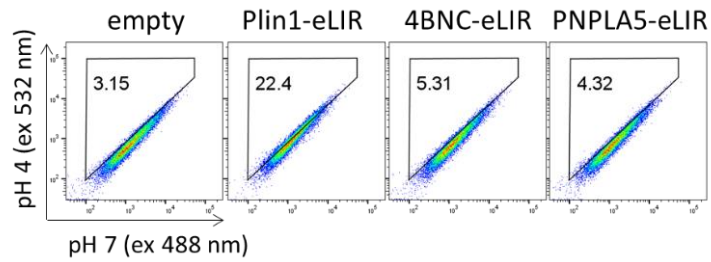
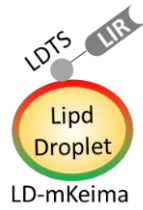
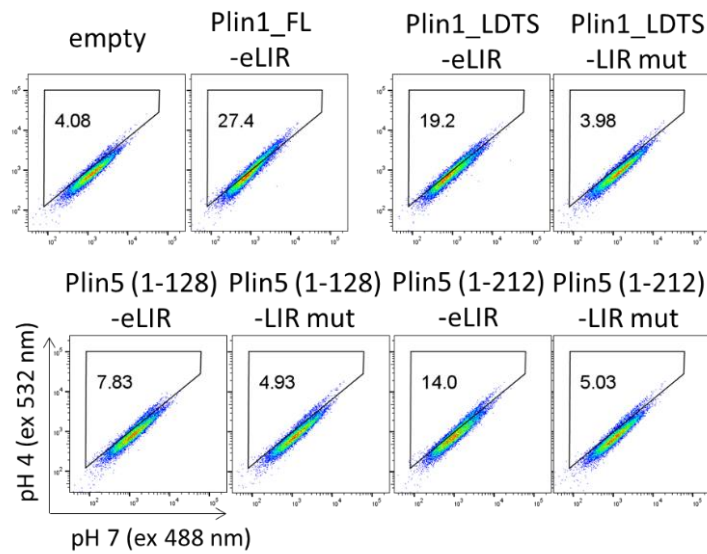
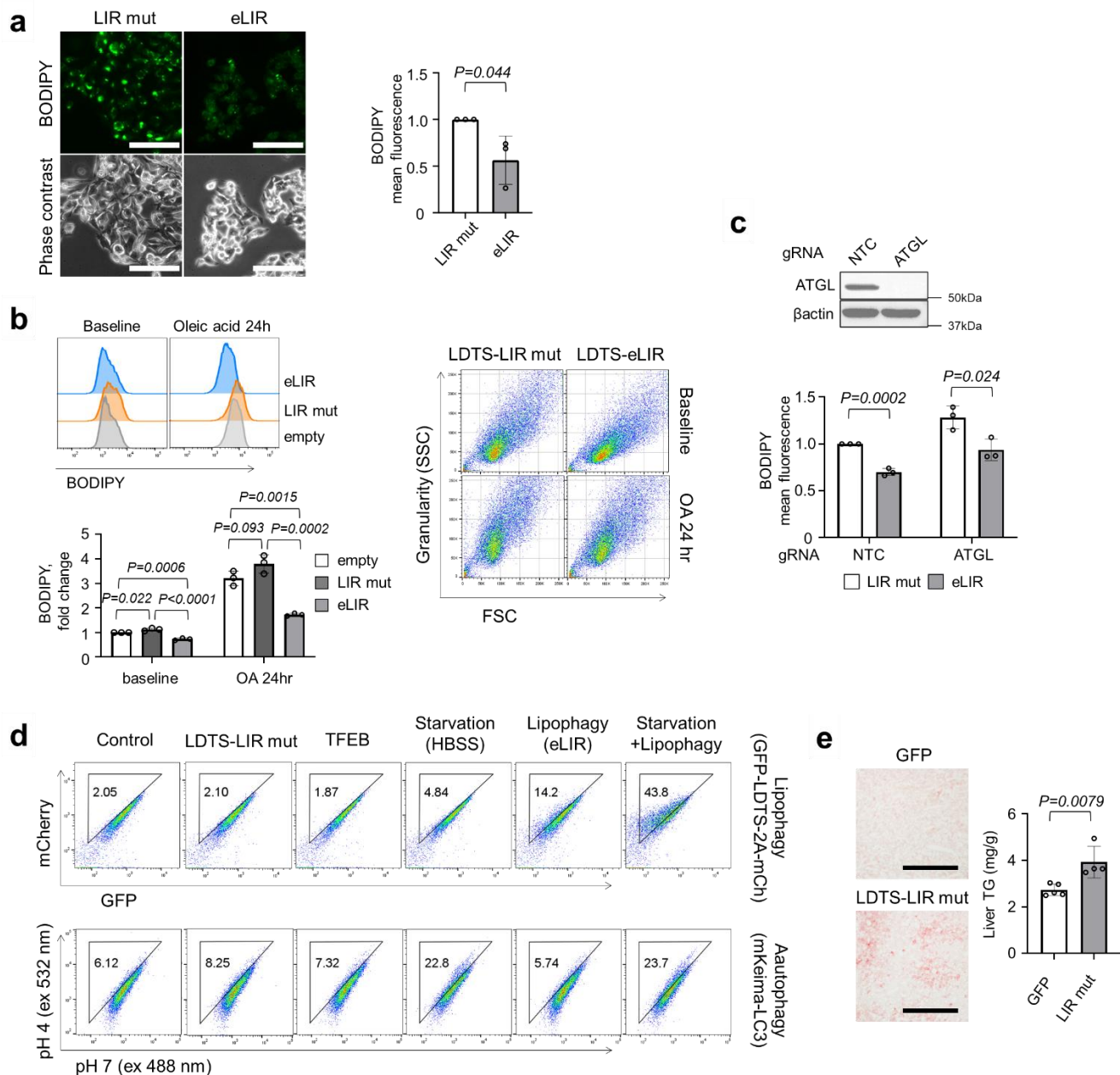


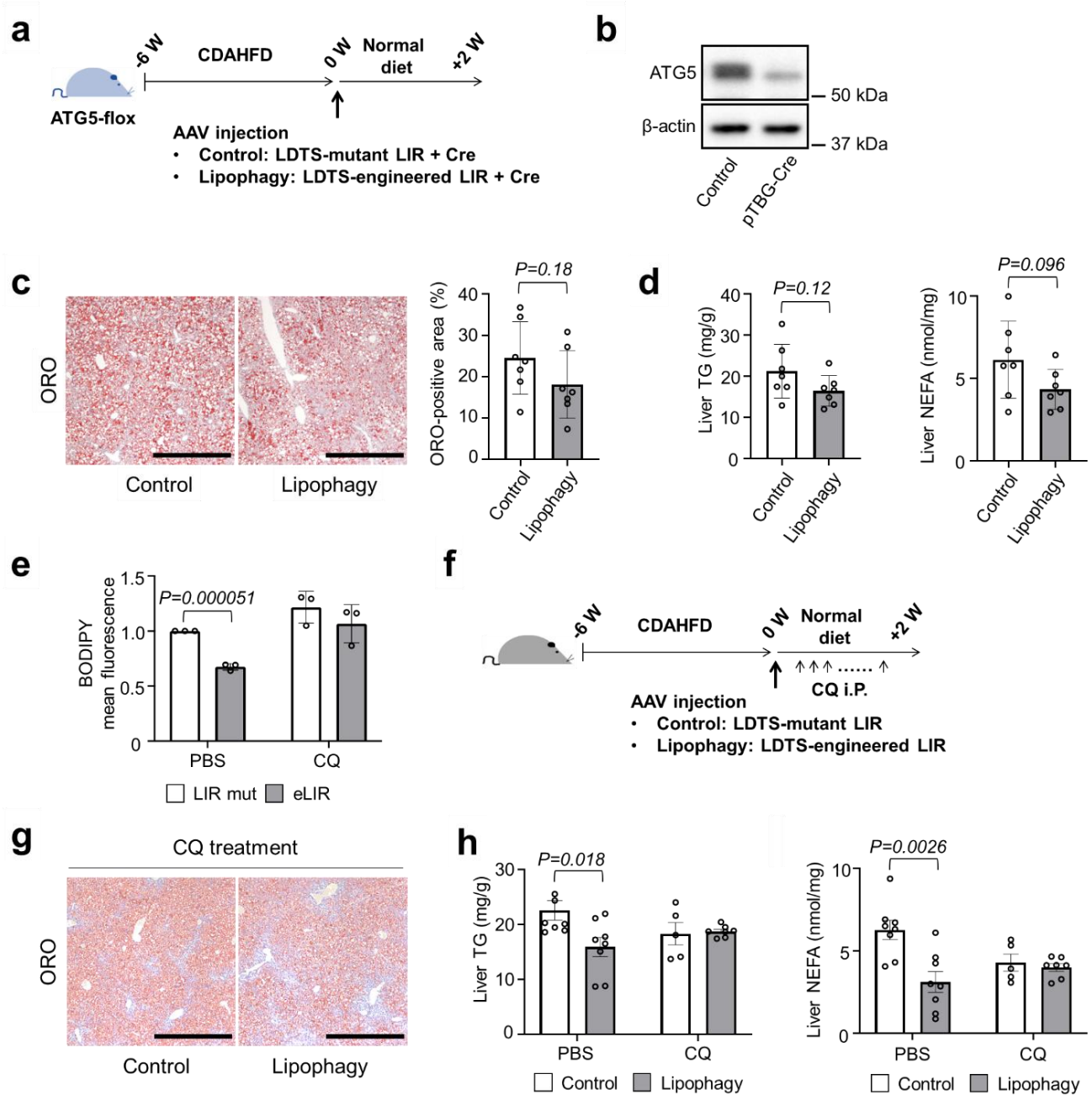
Supplementary Figure 1. Engineering LIR domain. (a) Autophagosome recruiting capacity of LC3 receptors assessed by mitophagy induction. Mitophagy level was quantified by mt-mKeima. (b) Domains of optineurin (OPTN) and interacting regions with binding partners (left). Identification of essential sequence for autophagosome recruiting capability (right). (c) Autophagosome recruiting capacity of phosphomimetic and tryptophan mutation (5EW) in full-length of OPTN in the SunTag system.

a**b**

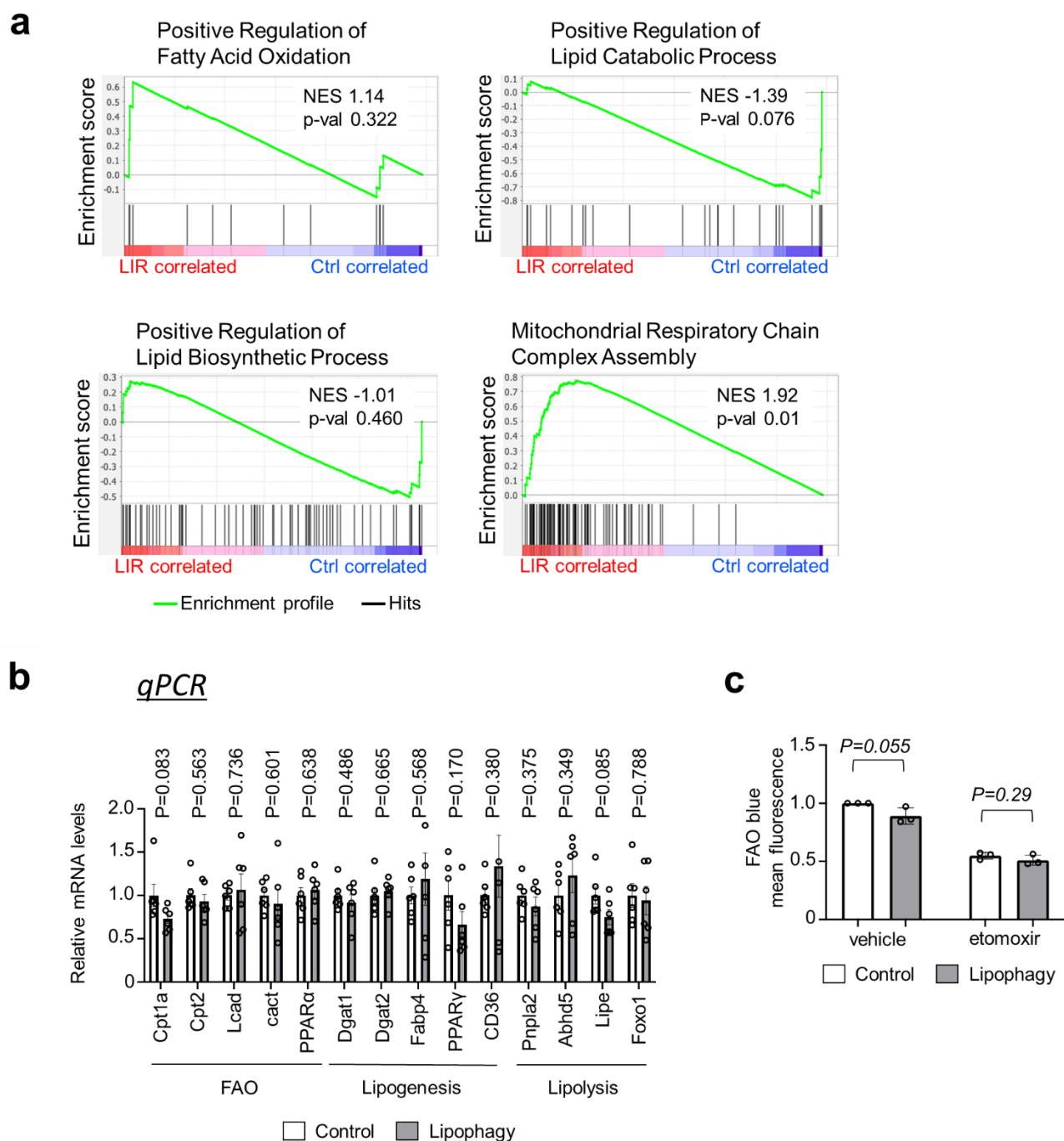
Supplementary Figure 2. Optimization of lipid droplet targeting signal. (a) Lipid droplet (LD) targeting capability of LD-related protein assessed by lipophagy induction in the fusion of engineered LIR (eLIR). (b) Essential sequence for LD-targeting signal (LDTS) of perilipin 1 and perilipin 5.



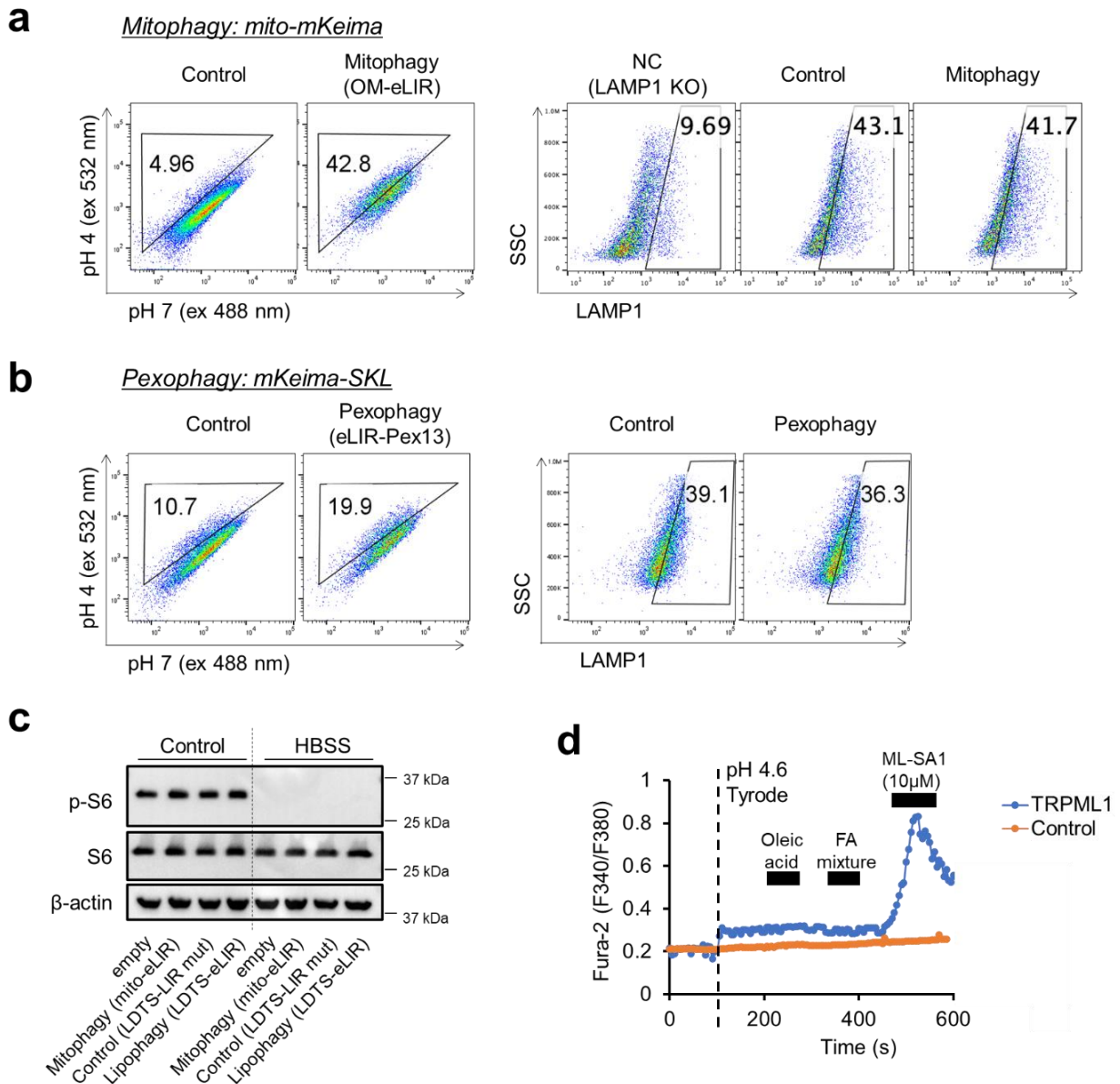
Supplementary Figure 3. Massive induction of lipophagy with LDTS-eLIR. (a) Fluorescence images of HepG2 cells stained with BODIPY after 24-hour incubation with oleic acid (left), and quantification of BODIPY fluorescence (right; $n=3$). Scale bars, 100 μm . (b) Quantification of BODIPY in HepG2 cells by flow cytometry (left; $n=3$), and the intracellular granularity reflecting the content of lipid droplets (right). (c) Immunoblots assessing the knockout of ATGL (top). Quantification of BODIPY by flow cytometry in ATGL knockout HepG2 cells treated with oleic acid for 24 hours (bottom; $n=3$). (d) The extent of lipophagy induction and concomitant autophagy activation with TFEB overexpression, starvation, and LDTS-eLIR-mediated lipophagy. (e) Oil red O (ORO) staining of liver sections (left) and liver TG content (right) 4 weeks after injection of AAV carrying GFP or LDTS-LIR mut in mice fed standard diet ($n=5$ GFP, $n=4$ LIR mut). Scale bars, 0.5 mm. All data are presented as mean \pm SD. P values calculated by two-sided unpaired t -test or one-way ANOVA with Tukey's multiple comparison test. Source data are provided as a Source Data file.



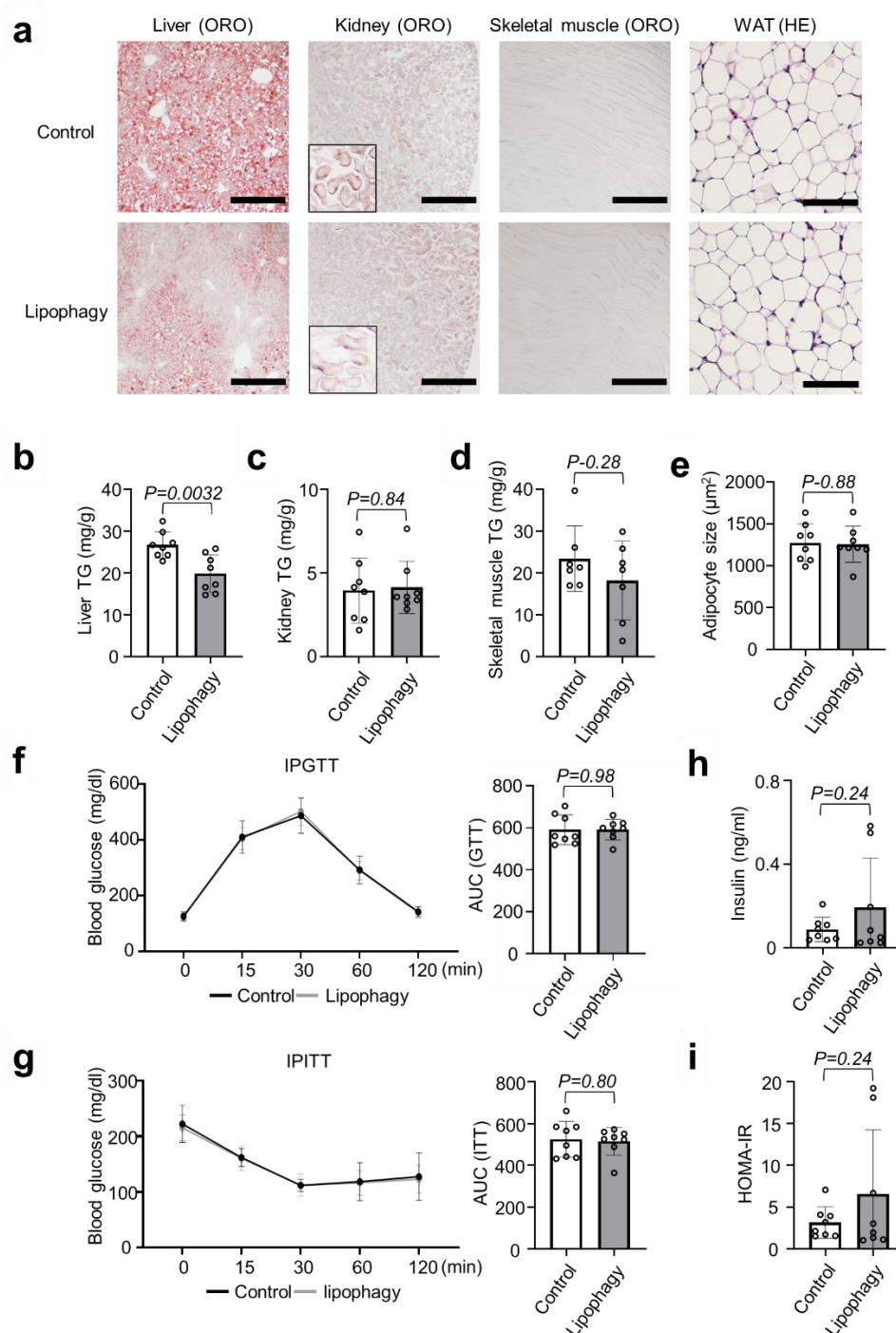
Supplementary Figure 4. Liver-specific ATG5 deletion and chloroquine treatment cancelled the effects of lipophagy. (a) Study protocol of NASH model with MCD diet, liver-specific ATG5 knockout and lipophagy induction. (b) Immunoblots assessing the expression of ATG5 in liver tissue isolated from ATG5-flox mice injected with AAV8 pTBG-Cre. (c) ORO staining of liver sections. Scale bars, 1 mm. (d) Liver TG and NEFA content. (n=7 for each group). (e) Quantification of BODIPY by flow cytometry in HepG2 cells treated with chloroquine (CQ, 25μM) and oleic acid for 24 hours (n=3). (f) Study protocol of NASH model with MCD diet, CQ treatment and lipophagy induction. (g) ORO staining of liver sections. Scale bars, 1 mm. (h) Liver TG and NEFA contents. (n=8 PBS groups, n=5 CQ+/control, n=7 CQ+/lipophagy). All data are presented as mean ± SD. *P* values calculated by two-sided unpaired *t*-test. Source data are provided as a Source Data file.



Supplementary Figure 5. Lipid metabolism in lipophagy-induced livers and HepG2 cells. (a) Gene set enrichment analysis for lipid metabolism in the RNA sequence of liver tissues related with Figure 2i,j. **(b)** Real-time quantitative PCR assessing the expression of genes associated with lipid metabolism in liver tissues (n=6 per group). **(c)** FAO activity in the cultured HepG2 cells. FAO blue is quenched fluorescent probe and metabolically activated by the sequential enzyme reactions of FAO (n=3). Data are presented as mean \pm SD. *P* values calculated by two-sided unpaired *t*-test. Source data are provided as a Source Data file.

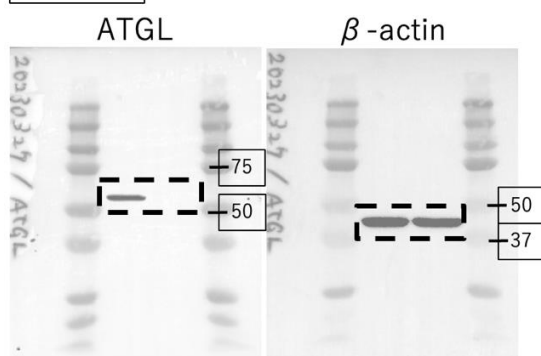


Supplementary Figure 6. Lysosomal exocytosis is independent of mTOR1 signal and nonesterified fatty acid. (a) Mitophagy induction by mitochondrial outermembrane-targeted eLIR was confirmed by flow cytometry for mt-mKeima in HepG2 cells (left). LAMP1 in the surface of HepG2 cells after induction of mitophagy (right). LAMP1 KO cells were used as a negative control. (b) Pexophagy induction by fusion protein of the localization motif of the peroxin Pex13 and eLIR was confirmed by flow cytometry for peroxisome-localized mKeima-SKL in HepG2 cells (left). LAMP1 in the surface of HepG2 cells after induction of pexophagy (right). (c) WB in lipophagy-induced cell under control or amino acid starvation. (d) Alteration in cytosolic Ca^{2+} was measured by the Fura-2 ratio (F340/F380) in 293T cells expressing TRPML1-L15L/AA-L577L/AA at low pH (pH 4.6) external solution. Cytosolic Ca^{2+} alteration wasn't observed in oleic acid or fatty acid mixture (arachidonic, linoleic, linolenic, myristic, oleic, palmitic and stearic acid). These experiments were repeated independently 3 times with similar results (a-d).

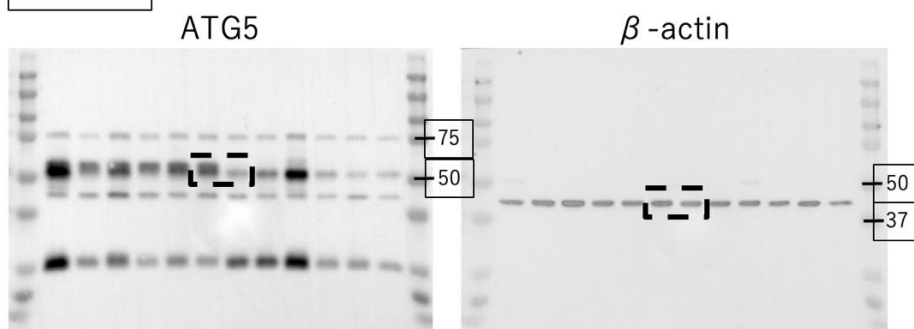


Supplementary Figure 7. Liver lipophagy wasn't associated with ectopic fat accumulation or abnormalities glucose metabolism. (a) Oil red O staining of liver, kidney and skeletal muscle sections from lipophagy-induced NASH model mice. Scale bars, 500 μm . Hematoxylin-eosin (HE) staining of WAT sections. Scale bars, 100 μm . (b-d) TG content in liver, kidney, skeletal muscle of lipophagy-induced NASH model mice. (e) Adipocyte size of epididymal adipose tissue. (f-i) Effects on the intraperitoneal glucose tolerance test (ipGTT), the intraperitoneal insulin tolerance test (ITT), the fasting serum insulin and HOMA-IR. All data are presented as mean \pm SD of $n=8$ per each group. P values calculated by two-sided unpaired t -test. Source data are provided as a Source Data file.

S Fig3 c



S Fig4 b



S Fig6 c

